Power uprates
and plant life extension

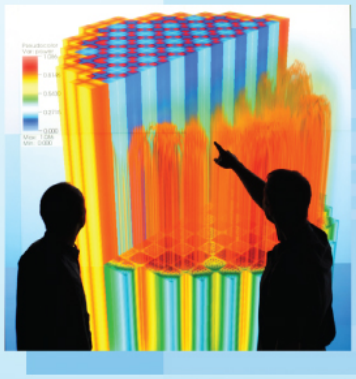

Engineering design
and analysis

Science-enabling
high performance
computing

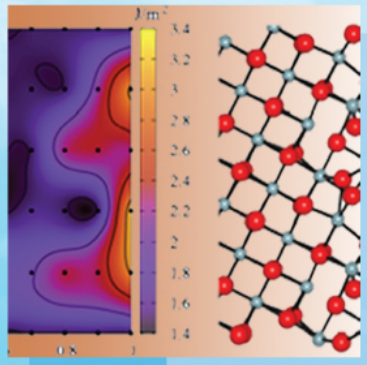

Fundamental science

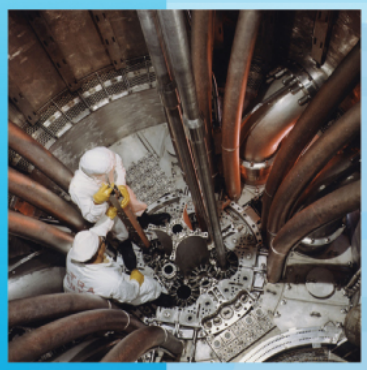

Plant operational data

Consortium for Advanced Simulation of LWRs

L3:MPO.CRUD.P6.01

D.A. Andersson, C. R. Stanek
LANL

December 18, 2012

U.S. DEPARTMENT OF ENERGY | Nuclear Energy

Mixing and non-stoichiometry in Fe-Ni-Cr-Zn-O spinel compounds: Density functional theory calculations

D. A. Andersson
Materials Science and Technology Division, Los Alamos National Laboratory, Los Alamos, NM 87545

C. R. Stanek
Materials Science and Technology Division, Los Alamos National Laboratory, Los Alamos, NM 87545
(Dated: December 18, 2012)

Density functional theory (DFT) calculations have been performed on $A^{2+}B_2^{3+}O_4^{2-}$ (where A^{2+}=Fe, Ni or Zn, B^{3+}=Fe or Cr and O^{2-}=O) spinel oxides in order to determine some of their thermodynamic properties. Mixing energies were calculated for Fe_3O_4-$NiFe_2O_4$, Fe_3O_4-$ZnFe_2O_4$, Fe_3O_4-$FeCr_2O_4$, $NiFe_2O_4$-$ZnFe_2O_4$, $NiFe_2O_4$-$NiCr_2O_4$, $NiCr_2O_4$-$FeCr_2O_4$, $ZnCr_2O_4$-$FeCr_2O_4$ and $ZnCr_2O_4$-$ZnFe_2O_4$ pseudo-binaries based on special quasi random (SQS) structures to account for the cationic disorder. The results generally agree with experimental data and the rule that two normal or two inverse spinel compounds easily form solid solutions, while inverse-normal spinel mixtures exhibit positive deviation from solid solution behavior (i.e. immiscibility). Even though systems such as $NiFe_2O_4$-$NiCr_2O_4$ and Fe_3O_4-$FeCr_2O_4$ obey this rule, they exhibit additional features with implications for the corresponding phase diagrams. In addition to mixing enthalpies, non-stoichoiemtry was also considered by calculating the energies of the corresponding defect reactions leading to A, B and O excess or deficiency. The most favorable non-stoichiometry reaction involves B^{3+} ions replacing A^{2+} ions and charge compensated by B^{3+} vacancies. This reaction is exothermic for most of the spinel compounds and leads to B and O excess. The spinels that contain both Fe^{2+} and Fe^{3+} ions (Fe_3O_4 and $CrFe_2O_4$), readily reacts to form O excess compounds via B vacancies charge compensated by holes or Fe^{3+} ions.

I. INTRODUCTION

Transition metal spinel oxides exhibit many interesting physical properties that are related to the versatility of the unfilled *d* electron orbitals and their bonding characteristics. This has inspired numerous studies of the fundamental spinel properties, including classical works on the Verwey transition controlling the carrier mobility in magnetite (Fe_3O_4)[3] and more recent studies on the effect of nano- and microstructure on the electronic and magnetic properties of $NiFe_2O_4$[4–7]. The continued interest in these materials is driven by their complex chemical, structural, magnetic and charge ordering characteristics, which lead to multiple degrees of freedom and the competition between these gives rise to a rich set of interesting properties that make these materials attractive for a range of technological applications[8].

In addition to being considered as functional materials, transition metal spinel oxides are formed as corrosion products on stainless steels and during internal oxidation, especially in high temperature applications. One example of the importance of spinel corrosion products is the formation of so-called CRUD on the cladding surface of nuclear fuels, which is also the application that motivated the present study. CRUD is an acronym for Chalk River Unidentified Deposit and refers to corrosion products that deposit on internal light water reactor (LWR) components, specifically on the upper parts of fuel rods where sub-cooled nucleate boiling occurs[9–11]. The major pressurized light water reactor (PWR) CRUD components are Ni and Fe oxides, which originate from corrosion of, e.g., steam generators. The structural materials used in steam generators are alloyed stainless steels with high concentration of Ni and Cr. Cr has an important role in corrosion of the steam generators, but it is usually not found in the CRUD deposits in any significant concentrations due to the very low Cr solubility in the coolant. In order to decrease the amount of Ni and Fe corrosion products, the coolant chemistry is modified by adding Zn, which is incorporated into the corrosive surfaces improving the properties of the protective oxide layer. This constrains the composition of interest to Fe, Ni, Cr and Zn spinels. The porous CRUD further attracts B containing precipitates, which, due to its neutron absorbing properties, shift the power distribution along the rod axis and leads to the CRUD Induced Power Shift (CIPS). This phenomenon is of increasing importance as nuclear plant operators are targeting higher power uprates and longer operating cycles. CRUD may also induce corrosion failure of the fuel pin via its interaction with the cladding. This is referred to as CRUD Induced Localized Corrosion (CILC) and is a consequence of increased temperatures at the cladding surface due to the low thermal conductivity of the CRUD layer. In boiling water reactors (BWR) the coolant chemistry, temperatures and materials selection is sufficiently different from PWRs that instead of $NiFe_2O_4$ the CRUD contains large quantities of $ZnFe_2O_4$ as well as other iron oxides, primarily Fe_2O_3.

In order to improve models of CRUD formation and growth, we have performed density functional theory (DFT) calculations on a number of Fe, Ni, Cr and Zn oxides relevant for either CRUD formation or corrosion processes. Specifically, the Fe_3O_4-$NiFe_2O_4$, Fe_3O_4-$ZnFe_2O_4$, Fe_3O_4-$FeCr_2O_4$, $NiFe_2O_4$-$ZnFe_2O_4$, $NiFe_2O_4$-$NiCr_2O_4$,

$NiCr_2O_4$-$FeCr_2O_4$, $ZnCr_2O_4$-$FeCr_2O_4$ and $ZnCr_2O_4$-$ZnFe_2O_4$ pseudo-binary mixing energies were calculated. Intrinsic and extrinsic defect reactions and the formation of non-stoichiometric Fe, Ni, Cr and Zn spinel compounds were also investigated, which included excess or deficiency of A^2, B^{3+} and O^{2-} ions. The calculated thermodynamic properties are compared to available experimental data. The results enable us to better understand both the formation of protective films on corrosion sources and the chemistry of the CRUD that is deposited on the fuel pins. Development of thermodynamic models of the Fe-Ni-Cr-Zn-O system also benefit from the DFT data presented in this work.

Many of the compounds that we have studied from thermodynamic and nuclear engineering perspectives have also received attention in spintronics and other emerging technologies[6,12–21] due to the electronic and magnetic properties of the transition metal spinel phases. Even though these topics are not specifically addressed in this study, some of our results are also relevant for these applications.

II. METHODOLOGY

The DFT calculations were performed with the Vienna Ab Initio Simulation Package (VASP)[22–24] using the projector augmented wave (PAW) method[25,26]. The Perdew-Burke-Ernzerhof (PBE) parameterization of the generalized gradient approximation (GGA) was used for the exchange-correlation potential[27]. Since standard GGA fails to capture the strongly-correlated nature of the 3*d* electrons in Fe, Ni, Cr and Zn oxides of present interest[28–40], an intra-band Hubbard U correction term was added to the standard DFT calculations according to the Dudarev implementation in VASP[41–44]. The Hubbard U method requires determination of the U (Hubbard U) and J (exchange) parameters. Since only the $U-J$ term enters the Dudarev Hubbard U model, a single value will be reported for $U-J$, which is henceforth referred to as U only. Literature U values were applied for all compounds. However, the U parameter has not been reported for all phases or compositions relevant to this study and, consequently, some simplifying assumptions have been made. The Ni U value ($U = 5.0$ eV for NiO) was taken from Ref. 45, Fe ($U = 4.3$ eV for tetrahedral and $U = 4.0$ eV for octahedral sites in Fe_3O_4 as well as $U = 3.7$ eV for FeO) from Ref. 28, Zn ($U = 7.1$ eV for ZnO) from Ref. 46 and 47 and Cr ($U = 3.2$ eV from Cr_2O_3) from Ref. 48. For some elements it is possible to find more than one U value in the literature, for example Janotti *et al.* used $U = 4.7$ eV for ZnO rather than $U = 7.1$ eV reported by Zhuo *et al.*[46,47]. It is expected that our qualitative conclusions will not be significantly impacted by use of slightly different U parameters. Even though some calculated numbers will change, such variation should not modify any of our qualitative conclusions. The exact U value may depend on, for example, the oxide stoichiometry and crystal structure[28], however these details have only been investigated for Fe oxides[28]. Consequently, the U values that have been determined for the dominant Ni and Zn oxide phases (monoxides) were applied to the spinel phases of present interest. Similarly, for Cr we used the U value for the Cr_2O_3 sesquioxide.

The DFT+U method provides increased accuracy for transition metal oxides, but for the corresponding metal phases it often performs worse than standard GGA calculations[36]. This is related to the *d* electrons changing from delocalized character in metals to more localized in the oxides. Consequently, we use the DFT+U method for the oxide and regular DFT for the metal phases. In order to be able to compare energies calculated within the two methods, as required to estimate many thermodynamic quantities, a common reference point must be established. This is achieved by applying the methodology recently developed by Jain *et al.*[36], which relies on experimental data for a few binary compounds to estimate the relation between regular DFT and DFT+U for each element.

$$\tilde{E}^{GGA+U} = E^{GGA+U} - \sum_M n_M \Delta E_M \qquad (1)$$

Here $\tilde{E}$ is the renormalized GGA+U energy, E^{GGA+U} is the original GGA+U energy, M represents the metal atoms that apply the GGA+U methodology, n_M is the number of such metal atoms in the compound and ΔE_M is the error in the binary oxide formation energy when GGA and GGA+U energies are used for the metal and oxides phases, respectively. In this study the FeO (Fe^{2+}), Fe_2O_3 (Fe^{3+}), ZnO, NiO and Cr_2O_3 formation energies were used for estimating ΔE_M of each atom and renormalizing the compound DFT+U values. By definition this approach will force the binary formation energies to agree perfectly with experiments, but Jain *et al.* showed that the methodology also significantly improves predictions for ternary and higher transition metal oxides[36]. The renormalization is only active when both oxide and metal phases are involved in reaction energies at the same time, such as for the calculation of standard oxide formation energies. If the energies of different oxide phases are compared this renormalization cancels out, which, for example, applies to mixing energies between two different spinel compounds.

The binding energy of O_2 molecules is significantly overestimated by DFT leading to errors in the compound formation energies. In order to minimize this problem we have applied the correction derived by Wang et al.[49]. The present thermodynamic analysis is only based on energy contributions to the free energy and thus best represents the materials behavior at low temperature. The formation energies were either calculated with respect to the most stable form of the pure elements under standard reference conditions (bcc Fe, fcc Ni, hcp Zn, bcc Cr and molecular O_2 gas) or the most stable binary oxide phases (FeO and Fe_2O_3 for Fe_3O_4, NiO and Fe_2O_3 for $NiFe_2O_4$, ZnO and Fe_2O_3 for $ZnFe_2O_4$, FeO

and Cr_2O_3 for $FeCr_2O_4$, ZnO and Cr_2O_3 for $ZnCr_2O_4$ and Cr_2O_3, FeO and Fe_2O_3 for $CrFe_2O_4$). The magnetic ground-states were used for Fe (ferromagnetic) and Cr (anti-ferromagnetic). Similarly, magnetism was accounted for in FeO, Fe_2O_3, Cr_2O_3 and ZnO (all anti-ferromagnetic). The mixing energies were calculated with the end-member spinel phases as reference. The same methodology was applied for estimating the energies of the intrinsic and extrinsic defect reactions.

All DFT calculations applied a plane-wave cut-off energy of 500 eV. For the spinel phases either $4 \times 4 \times 4$ or $6 \times 6 \times 6$ Monkhorst-Pack k-point meshes[50] with a Gaussian smearing of 0.05 eV were used. The band gaps and electronic density of states were calculated using the modified tetrahedral method of Blöchl[51]. Calculations of all unary and binary phases applied k-point meshes that were converged to at least the same accuracy as the spinel compounds. The structure models were minimized with respect to cell volume and shape as well as atomic positions in order to yield zero external pressure and vanishing forces for every atom (< 0.02 eV/Å). Spin-polarized calculations were applied for all compounds and the equilibrium (lowest energy) spin arrangement was determined by calculating total energies for a number of different ferromagnetic and anti-ferromagnetic initial structures. Intrinsic defects were modeled with both regular and charged supercell calculations. The latter approach enables us to capture the relevant charge states of Frenkel and Schottky defects as well as for the extrinsic defect reactions. The charged supercell calculations applied the standard DFT methodology of compensating the electron excess/defiencancy with a homogeneous background charge[52,53]. The defect energies were corrected for the leading errors arising due to interaction between image charges in the supercells.

The generic spinel compound is written $A^{2+}B_2^{3+}O_4^{2-}$[54,55] and its conventional unit cell contains 56 atoms, as illustrated in Fig. 1. In normal spinels the divalent A^{2+} ions occupy tetrahedral sites and the trivalent B^{3+} ions octahedral sites, while in inverse spinels the A^{2+} ions mix with B^{3+} ions on octahedral sites and conversely B^{3+} ions occupy the tetrahedral sites. Various degrees of inversion are possible and full inversion corresponds to only B^{3+} ions in tetrahedral positions. The A^{2+} and B^{3+} ions on octahedral sites are randomly distributed at high temperature, but they form ordered compounds at low temperature. This is usually associated with a transformation from cubic to lower symmetry structures[56]. The disordered inverse spinel structures as well as solid solutions such as $Ni_{1-x}Zn_xFe_2O_4$ were modeled using special quasi random (SQS) structures[57,58]. We used the SQS structures derived by Jiang *et al.* to capture inversion in MgX_2O_4 (X = Al, Ga, In) spinels[59]. The 56 atom cell used for the SQS structures is not large enough to reach very high accuracy for the atomic correlation functions[59]. However, the sensitivity of the mixing energies with respect to the detailed atomic distribution was tested for a number of cases and any variation was too small to impact the present conclusions. At very high temperatures the A and B ions would fully disorder between the tetrahedral and octahedral sites. We did not attempt to model this state, since we are not concerned with properties in that temperature range. The calculation of defect properties involve interstitial species that may occupy either the empty tetrahedral or octahedral sites of the spinel structure.

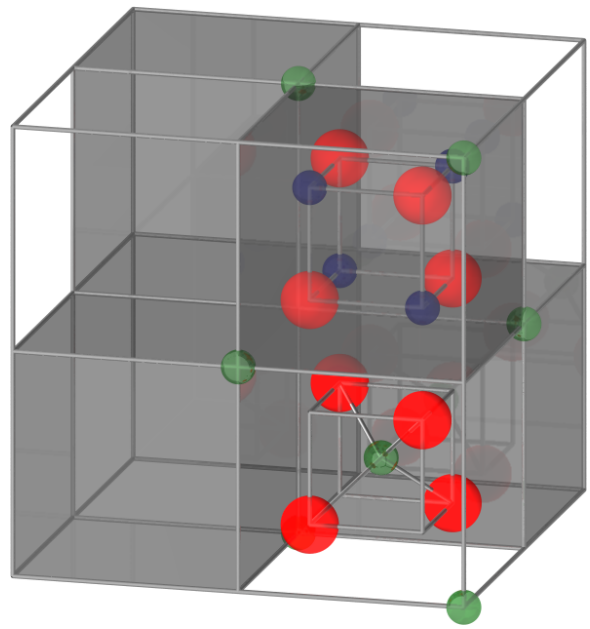

FIG. 1. The primitive tetragonal and cubic unit cells of spinel (reproduced from[54], where red atoms are oxygen, green are A and blue are B cations. The atomic structure repeats according to the shading of the 1/8 cubes shown.

III. RESULTS AND DISCUSSION

A. Electronic and magnetic properties of Fe, Ni, Cr and Zn spinels

In order to reliably calculate thermodynamic properties of Fe, Ni Cr and Zn spinels, it is necessary to first establish that the DFT methodology captures the basic electronic structure of these compounds. All of the Fe, Ni, Cr and Zn spinel compounds considered exhibit rather complex magnetic structures due to the localized spins on the transition metal ions[60]. In most of these spinels the spins localized on the metal ions are ordered in an anti-ferromagnetic pattern[61–67]. Depending on the constituent metal ions, this gives rise to either anti-ferromagnetism with zero net magnetic moment or ferrimagnetism with a finite total magnetic moment that arises from unbalanced spin up and down contributions. For each compound all major spin ordering possibilities were investigated, but the formation energy is only re-

ported for the most stable magnetic structure. In the inverse Fe_3O_4 and $NiFe_2O_4$ spinels the Fe^{3+} ions on tetrahedral sites are anti-ferromagnetically arranged with respect to the both the Ni^{2+} and Fe^{3+} ions on the octahedral sites, which agrees with experiments[62,67] and existing DFT studies[31,35,68]. Among the normal spinels $NiCr_2O_4$ and $CrFe_2O_4$ exhibit anti-ferromagnetic alignment between the tetrahedral and octahedral sites, similar to the inverse spinels[66]. The remaining $ZnFe_2O_4$, $CrFe_2O_4$, $FeCr_2O_4$, $ZnCr_2O_4$ compounds instead favor anti-ferromagnetic arrangement between the trivalent ions on the octahedral sites. Accounting for the correct magnetic ordering has significant impact on the calculated formation energies for, in particular, the inverse spinel compounds. This is evidenced by the fact that the Néel temperatures for Fe_3O_4 and $NiFe_2O_4$ are high (848 K[61] and 858 K[62], respectively), thus indicating strong magnetic interactions and ordering energies. On the other hand the Néel temperatures for the normal $ZnFe_2O4$ and $ZnCr_2O_4$, $FeCr_2O_4$ and $NiCr_2O_4$ spinels are as low as 10.5 K[63], 13 K[64], 80 K[65] and 74 K[66], respectively. The ground-state magnetic configuration is listed in Table I and the DFT classification is in good agreement with the experimental findings. All point defects were modeled assuming that the magnetic configuration does not change from the defect-free compound, i.e. the the magnetic configuration of the defect-free compound was used to initialize the DFT calculations for the defect-containing systems. The magnetic properties of the mixed spinel oxides were assumed to follow similar rules. For the compounds with low Néel temperatures, some scatter is obtained due to the low energy scale of magnetic interactions and the corresponding coupling between the distribution of cations and magnetic moments.

The electronic structure of the spinel compounds was also investigated. The calculated band gaps are reported in Table I. For Fe_3O_4 a gap of 0.75 eV is predicted in the minority spin band between occupied and unoccupied Fe d states, which agrees fairly well with other theoretical studies[69]. The reader is directed to other studies for a detailed analysis of the Fe_3O_4 bonding characteristics and electronic structure[69]. The $NiFe_2O_4$ gap is 1.63 eV and it divides the O $2p$ dominated valence band from the Fe d dominated lower part of the conduction band. The $CrFe_2O_4$ band structure is rather similar to Fe_3O_4, but it exhibits a slightly higher band gap of 1.23 eV. The largest band gap is obtained for $ZnCr_2O_4$ (2.82 eV). For this compound both the top of the valence band and the bottom of the conduction band are dominated by Cr d states. The corresponding states for $ZnFe_2O_4$ involve Fe d states and larger contributions from O $2p$ orbitals in the valence band, and the band gap is somewhat smaller (1.68 eV). For $NiCr_2O_4$ the top of the valence band is dominated by Cr d states and the bottom of the conduction band by Ni d states. The band gap is 1.86 eV. $FeCr_2O_4$ has a gap of 2.09 eV in the minority spin band, which primarily involves Fe d states in the valence band and Cr d states in the lower part of the conduction band. Further analysis of the spinel bonding characteristics is beyond the scope of the present study.

B. Thermodynamic properties of Fe, Ni, Cr and Zn spinels

Table I summarizes the calculated formation energies (E_f) and volumes (V) of Fe_3O_4, $NiFe_2O_4$, $ZnFe_2O_4$, $NiCr_2O_4$, $FeCr_2O_4$, $ZnCr_2O_4$ and $CrFe_2O_4$ spinels as well as the corresponding reference values (where available) from Refs. 70–75. For each compound the properties were calculated for normal, inverse ordered and inverse disordered spinels. Even though calculations were performed for all possible spinels in the Fe-Ni-Cr-Zn system, data is only reported for compounds that satisfy the formal spinel valence rules since they are the only ones that may occur as stable compounds. In these spinel compounds Ni and Zn always act as divalent ions, while Fe and Cr exhibit mixed valence properties and exist in both divalent and trivalent forms. However, even though Cr ions may act as Cr^{2+}, they rather strongly prefer the Cr^{3+} state. For each spinel compound there are two calculated formation energies. The first one applies the most stable unary phases and the second one the most stable oxide phases as reference states, respectively. Negative formation energies imply that the spinel phase is stable with respect to the reference phases.

In agreement with experiments and existing theoretical investigations Fe_3O_4 and $NiFe_2O_4$ are predicted to be inverse spinels[40,68,71,72]. Both compounds have an ordered arrangement of cations as the most stable state. For Fe_3O_4 we were not able to investigate the normal spinel or the inverse disordered state, since the distribution of Fe^{2+} and Fe^{3+} ions is determined self-consistently in the DFT calculations, which implies that they will (typically) reach the lowest energy ordered inverse configuration. $ZnFe_2O_4$, $NiCr_2O_4$, $FeCr_2O_4$ and $ZnCr_2O_4$ are all predicted to be normal spinels, which is consistent with experiments for the first three compounds[73–75]. Of these $ZnFe_2O_4$ has the lowest disordering energy equal to 0.15 eV per formula unit. However, even for this case the temperature must be high in order to reach any significant degree of inversion and the other compounds can be considered as almost perfect normal spinels. $CrFe_2O_4$ exhibits the most complex properties of all the compounds that we investigated. The reason is that it contains two transition metal ions that both have mixed valence character. We predict the lowest energy state to be a normal spinel with Fe^{2+} ions on the tetrahedral sites and a mixture of Cr^{3+} and Fe^{3+} ions on the octahedral sites. The formation energy of the compound with the Cr ions on the tetrahedral sites (ordered) is 1.24 eV higher. This compound is an inverse spinel with the Cr ions acting as Cr^{3+} ions. The disordered inverse spinel is even higher in energy and for this case the solution is only partially inverse, i.e. some of the Cr ions on tetrahedral sites have Cr^{2+} character. All spinels have negative forma-

tion energies with respect to the pure elements as well as with respect to the oxide reference states. This suggests that they are thermodynamically stable, however as explained in Sec. III C many of the spinel compounds react exothermically to form non-stoichiometric compounds. The DFT calculations slightly overestimate the volume of the spinel compounds.

Next, the Fe_3O_4-$NiFe_2O_4$, Fe_3O_4-$ZnFe_2O_4$, Fe_3O_4-$FeCr_2O_4$, $NiFe_2O_4$-$ZnFe_2O_4$, $NiFe_2O_4$-$NiCr_2O_4$, $NiCr_2O_4$-$FeCr_2O_4$, $ZnCr_2O_4$-$FeCr_2O_4$ and $ZnCr_2O_4$-$ZnFe_2O_4$ mixing energies were calculated for both normal and inverse spinel compounds. The distribution of, e.g., Ni ions in $Ni_yFe_{3-y}O_4$ was modeled using SQS structures. For some cases SQS structures were not available and simplified models were used, however the results were not very sensitive to this simplification. The results are summarized in Figs. 2, 3 and 4.

Rules derived from experimental experience state that two normal or two inverse spinel compounds easily form solid solutions, while normal and inverse spinels exhibit limited solubility or are simply immiscible[76]. This is generally confirmed by our calculations. The $FeCr_2O_4$-$NiCr_2O_4$, $FeCr_2O_4$-$ZnCr_2O_4$ and $ZnCr_2O_4$-$ZnFe_2O_4$ pseudo-binary systems all exhibit mixing energies that are near zero. Nevertheless, there are some features that may effect the solution properties. For example, $ZnCr_2O_4$-$ZnFe_2O_4$ has almost parabolic shape with a minimum at $y_{Zn}/(y_{Fe} + y_{Cr}) = 0.5$, except for low Cr content where the mixing energy is positive. Both $FeCr_2O_4$-$NiCr_2O_4$ and $FeCr_2O_4$-$NiCr_2O_4$ exhibit slightly positive mixing energies near to the Fe poor region and slightly negative values near to the Fe rich region. There is some irregularity in the mixing energy curves for many of these compounds, which is likely caused by small differences in structure or magnetic correlation functions. Recall that the magnetic ordering temperatures are fairly low in the end-member compounds.

$NiFe_2O_4$ is an inverse spinel and $ZnFe_2O_4$ is a normal spinel and, as expected, mixing energies are positive with the maximum shifted towards the $NiFe_2O_4$ region. At the maximum there is a transition between inverse and normal spinel ordering. The calculated positive mixing energies are in good agreement with the measured miscibility gap[62]. The experimental data also indicate that the maximum of the miscibility gap is shifted towards the $NiFe_2O_4$ rich region. In the neighborhood of the transition point between normal and inverse spinels one could expect a partially inverse spinel to be preferred, but the DFT calculations show that it is not the case. Either the normal or the inverse spinel is the most stable compound. However, the exact transition point, for which one would expect close to equal distribution between normal and inverse sites, could not be tested within the present spinel supercell.

$NiFe_2O_4$-$NiCr_2O_4$ exhibits a more interesting and to some extent unexpected behavior. Even though $NiCr_2O_4$ is a normal and $NiFe_2O_4$ is an inverse spinel, $NiCr_2O_4$ has negative solution energy in $NiFe_2O_4$ up to $NiFe_1Cr_1O_4$, i.e. when the Cr ions have filled all available octahedral sites and starts filling tetrahedral sites. Since the Cr^{3+} ions in $NiCr_2O_4$ prefer octahedral sites it is not surprising that they easily dissolve into the same sites in $NiFe_2O_4$. Similarly, since the tetrahedral sites are unfavorable for Cr^{3+} ions the mixing energy is expected to increase at that point. The measured $NiFe_2O_4$-$NiCr_2O_4$ phase diagram[77] indicates an almost symmetric miscibility gap, which is at least in partial disagreement with the calculated mixing energies. However, the calculations agree very well with the phase diagram obtained by Park et al.[78].

Fe_3O_4 and $NiFe_2O_4$ are both inverse spinels and have negative mixing energies with a minimum at $Ni_{0.75}Fe_{2.25}O_4$. Existing phase diagrams show that at intermediate and high temperature $NiFe_2O_4$ may dissolve excess Fe with respect to Fe_2O_3. At low temperature the ordered inverse spinel compound appears as a line compound in both experimental phase diagrams[79] and according to the present DFT calculations. Corrosion studies have reported preferred $Ni_{1-x}Fe_{2+x}O_4$ compositions near $x \approx 0.3$[80–82], which is consistent with the minimum of the mixing energy obtained from the DFT calculations. Fe_3O_4-$ZnFe_2O_4$ and Fe_3O_4-$FeCr_2O_4$ are both mixtures between inverse and normal spinels. Fe_3O_4-$ZnFe_2O_4$ exhibits positive mixing energies throughout the full composition range, while Fe_3O_4-$FeCr_2O_4$ has positive mixing energies between $y_{Cr}/(y_{Cr} + y_{Fe}) = 0.0625$ and 0.5 (y_X is the atomic fraction of the respective atoms). The negative mixing energies in the $FeCr_2O_4$ rich region can be explained in a similar way to the $NiFe_2O_4$-$NiCr_2O_4$ system. Recall that $CrFe_2O_4$, which represents the $y_{Cr}/(y_{Cr} + y_{Fe}) = 0.5$ midpoint, is a normal spinel and the $CrFe_2O_4$-$FeCr_2O_4$ part of the mixing energy curve is thus expected to be close to an idea solution, while the Fe_3O_4-$CrFe_2O_4$ part is not, since it represents a mixture between an inverse and normal spinel. These observations agree with the results in Fig. 4 and they also agree with the Cr rich compounds observed in corrosion studies[80–82].

C. Thermodynamic properties of non-stoichiometric Fe, Ni, Cr and Zn spinels

The possibility of forming non-stoichiometric compounds was investigated by calculating the formation energy of metal and oxygen vacancies and interstitials that comprise the possible defect reactions. First we consider the individual defects, then intrinsic processes and finally non-stoichoiemtry reactions. The results presented here only include the most favorable vacancy and interstitial reactions. For example, in Fe_3O_4 it is much easier to create Fe vacancies on octahedral than on tetrahedral sites (0.46 eV vs. 1.48 eV). The same relation holds for Fe vacancy formation in other inverse spinels ($NiFe_2O_4$). The spinel crystal structure has two different interstitial sites,

	E_f Normal (eV/f.u.)	E_f Inv. Ord. (eV/f.u.)	E_f Inv. Dis. (eV/f.u.)	E_f Exp., 298 K (eV/f.u.)	Magn.
Fe_3O_4	N/A	-11.59	-11.59	-11.59[70] (inv.)	ferrimagnetic
$NiFe_2O_4$	-10.48/0.57	-11.24/-0.19	-11.18/-0.13	-11.24[70] (inv.)	ferrimagnetic
$ZnFe_2O_4$	-12.07/-2.83	-11.98/-2.73	-11.92/-2.68	-12.22[70] (norm.)	anti-ferromagnetic
$NiCr_2O_4$	-14.21/-2.79	-13.28/-1.86	-13.23/-1.81	-14.24[70] (norm.)	ferrimagnetic
$FeCr_2O_4$	-15.11/-3.36	-13.64/1.89	-13.60/-1.85	-14.58[70] (norm.)	ferrimagnetic
$ZnCr_2O_4$	-15.79/-3.25	-13.98/-1.45	-13.94/-1.41	N/A	anti-ferromagnetic
$CrFe_2O_4$	-13.37/-1.81	-10.99/0.57	-11.87/-0.31	N/A	anti-ferromagnetic
	V Normal (Å^3/f.u.)	V Inv. Ord. (Å^3/f.u.)	V Inv. Dis. (Å^3/f.u.)	V Exp. (Å^3/f.u.)	Band gap (eV)
Fe_3O_4	N/A	76.7	76.7	73.62[71]	0.75
$NiFe_2O_4$	91.0	74.0	74.3	72.43[72]	1.63
$ZnFe_2O_4$	75.5	74.6	74.8	75.07[73]	1.68
$NiCr_2O_4$	75.2	74.1	74.1	71.57[74]	1.86
$FeCr_2O_4$	77.3	76.8	77.4	73.82[75]	2.09
$ZnCr_2O_4$	74.2	74.6	74.9	N/A	2.82
$CrFe_2O_4$	76.2	85.7	77.8	N/A	1.23

TABLE I. The formation energy (E_f) and volume (V) per formula unit (f.u.) of normal, inverse ordered and inverse disordered spinel compounds with respect to the most stable unary phases (first entry) or the most stable binary oxide phases (second entry). Where available the experimental volume and formation energy is also listed together with the preferred spinel ordering (normal or inverse). The ground-state magnetic structure (Magn.) and band gap for the most stable compounds are also listed.

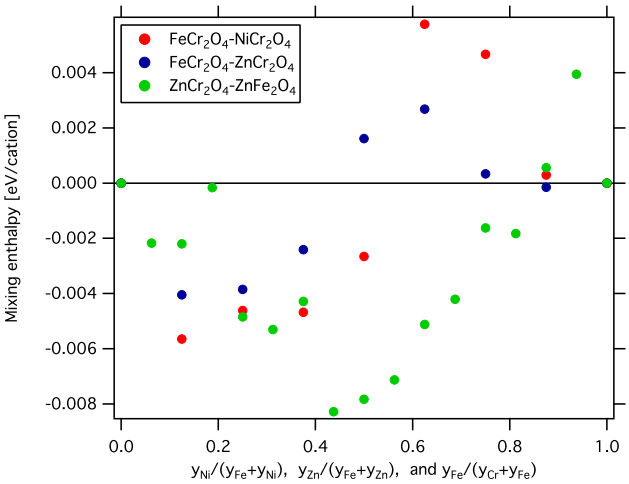

FIG. 2. $FeCr_2O_4$-$NiCr_2O_4$ (red), $FeCr_2O_4$-$ZnCr_2O_4$ (blue) and $ZnCr_2O_4$-$ZnFe_2O_4$ (green) mixing energies for normal spinels. The first compound (e.g. $FeCr_2O_4$ in $FeCr_2O_4$-$NiCr_2O_4$) is on the left hand side of the plot and the second one (e.g. $NiCr_2O_4$) is on the right hand side. y_{Fe}, y_{Cr}, y_{Ni} and y_{Zn} denote the atomic fraction of the respective atoms.

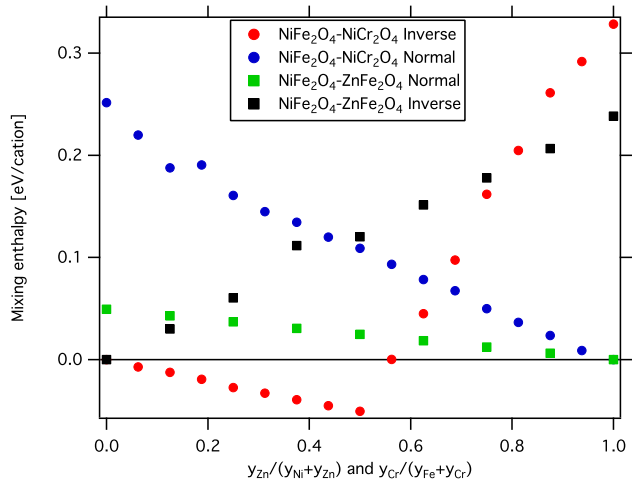

FIG. 3. $NiFe_2O_4$-$ZnFe_2O_4$ (green=normal and black=inverse squares) and $NiFe_2O_4$-$NiCr_2O_4$ (red=inverse and blue=normal circles) mixing energies. The first compound (e.g. $NiFe_2O_4$ in $NiFe_2O_4$-$ZnFe_2O_4$) is on the left hand side of the plot and the second one (e.g. $ZnFe_2O_4$) is on the right hand side. y_{Fe}, y_{Cr}, y_{Ni} and y_{Zn} denote the atomic fraction of the respective atoms.

one octahedral and one tetrahedral site. Results of DFT calculations predict the octahedral site to be the most stable one for Fe and oxygen interstitials. The metal ions are slightly displaced from the centre of the octahedral hole. The site preference is not as strong for Ni, Zn or Cr ions.

The thermodynamic properties of the spinel phases are defined by the intrinsic and extrinsic defect reactions listed below. The intrinsic defects for the $A^2B_2^{3+}O_4^{2-}$ spinel include the cation anti-sites (reaction 2), Schottky (reaction 3) and Frenkel reactions (reactions 4, 5 and 6). The first reaction is related to the degree of inversion. For this reason the anti-site defect energy is not reported for the inverse spinel compounds, since they are fully inverse in their most stable state.

$$A_A^x + B_B^x \rightleftharpoons B_A^\bullet + A'_B \qquad (2)$$

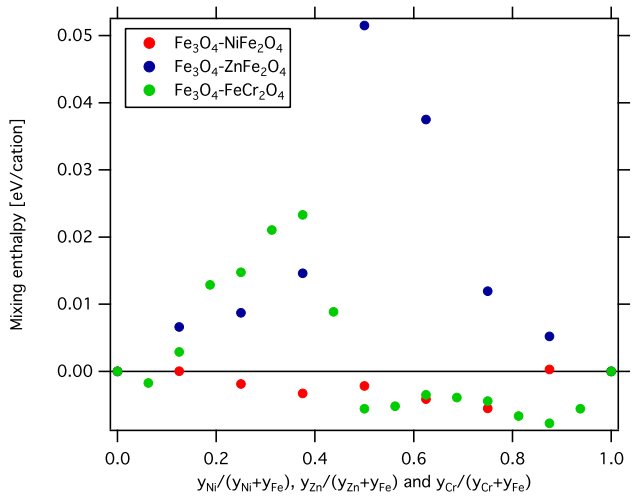

FIG. 4. Fe_3O_4-$NiFe_2O_4$ (red), Fe_3O_4-$ZnFe_2O_4$ (blue) and Fe_3O_4-$FeCr_2O_4$ (green)mixing energies. The first compound (e.g. Fe_3O_4 in Fe_3O_4-$NiFe_2O_4$) is on the left hand side of the plot and the second one (e.g. $NiFe_2O_4$) is on the right hand side. y_{Fe}, y_{Cr}, y_{Ni} and y_{Zn} denote the atomic fraction of the respective atoms.

$$A_A + 2B_B + 4O_O \rightleftharpoons V_A'' + 2V_B''' + 4V_O^{\bullet\bullet} + AB_2O_4 \quad (3)$$

$$A_A^x + V_I^x \rightleftharpoons V_A'' + A_I^{\bullet\bullet} \quad (4)$$

$$B_B^x + V_I^x \rightleftharpoons V_B''' + B_I^{\bullet\bullet\bullet} \quad (5)$$

$$O_O^x + V_I^x \rightleftharpoons V_O^{\bullet\bullet} + O_I'' \quad (6)$$

The intrinsic defect reaction energies were estimated from charged supercell calculations of the individual vacancy and interstitial defects. This is necessary in order to avoid, for example, oxygen interstitials (O_I'') to be associated with two holes ($2h^\bullet$) or Fe^{3+} ions in the supercells, which are not components of the intrinsic defect reactions. The latter charge compensation and equivalent mechanisms for other defects are, in principle possible, but are always higher in energy than the reactions in Eqs. 3, 4, 5 and 6. Energies for anti-site, Frenkel and Schottky defects are collected in Table II. Anti-site defects have the lowest reaction energies for all compounds and the minimum of all compounds considered is obtained for $ZnFe_2O_4$, which is consistent with the energy difference between normal and inverse spinels (see Table I). With respect to the anti-site defects all other defect energies are relatively high, except for Fe^{2+} Frenkel pairs in Fe_3O_4 (1.87 eV). Not including anti-sites, Fe Frenkel pairs are the most favorable intrinsic defects for Fe_3O_4, $ZnFe_2O_4$ and $FeCr_2O_4$. Out of these, only $ZnFe_2O_4$ involves Fe^{3+} ions. Similarly, Ni Frenkel pairs are preferred for $NiCr_2O_4$ and for $NiFe_2O_4$.

The same approach was used to calculate the energies of extrinsic defect reactions leading to excess or deficiency of A, B or O ions (non-stoichiometry). Holes ($h^\bullet$) and electrons (e') were either modeled in separate supercells (as defined in the reactions below) or contained in the same supercell as the corresponding atomic defects. The latter case corresponds to clustering and it is separated from the first case by the label 'c' in Table III. In order to qualitatively analyze the mechanisms by which these compounds deviate from stoichiometry, we here list the plausible reactions. The implications of these reactions on A, B and O excess or deficiency are discussed below and illustrated in Fig. 5.

$$2AO + 2B_B^x + O_O^x \rightleftharpoons 2A_B' + V_O^{\bullet\bullet} + B_2O_3 \quad (7)$$

$$3AO + 3V_I^x + 2B_B^x \rightleftharpoons 3A_I^{\bullet\bullet} + 2V_B''' + B_2O_3 \quad (8)$$

$$AO + 2V_I^x \rightleftharpoons A_I^{\bullet\bullet} + O_I'' \quad (9)$$

$$AO + 2AB_2O_4 + V_I^x \rightleftharpoons A_I^{\bullet\bullet} + 2e' + \frac{1}{2}O_2 \quad (10)$$

$$A_A^x + O_O^x \rightleftharpoons V_A'' + V_O^{\bullet\bullet} + AO \quad (11)$$

$$3A_A^x + 2V_I^x + B_2O_3 \rightleftharpoons 3V_A'' + 2B_I^{\bullet\bullet\bullet} + 3AO \quad (12)$$

$$2AB_2O_4 + A_A^x + \frac{1}{2}O_2 \rightleftharpoons V_A'' + 2h^\bullet + AO \quad (13)$$

$$4B_2O_3 + 3A_A^x \rightleftharpoons 2B_A^\bullet + V_A'' + 3AB_2O_4 \quad (14)$$

$$8B_2O_3 + 6A_A^x + 2B_B^x \rightleftharpoons 6B_A^\bullet + 2V_B''' + 6AB_2O_4 \quad (15)$$

$$3B_2O_3 + 2A_A^x + B_B^x \rightleftharpoons 2B_A^\bullet + O_I'' + 2AB_2O_4 \quad (16)$$

$$BO + A_A^x = B_A^x + AO \quad (17)$$

$$B_2O_3 + 5V_I^x \rightleftharpoons 2B_I^{\bullet\bullet\bullet} + 3O_I'' \quad (18)$$

$$6AB_2O_4 + B_2O_3 + 2V_I^x \rightleftharpoons 2B_I^{\bullet\bullet\bullet} + 6e' + \frac{3}{2}O_2 \quad (19)$$

$$2B_B^x + 3O_O^x \rightleftharpoons 2V_B''' + 3V_O^{\bullet\bullet} + B_2O_3 \quad (20)$$

$$2B_B^x + 3V_I^x + 3AO \rightleftharpoons 2V_B''' + 3A_I^{\bullet\bullet} + B_2O_3 \quad (21)$$

$$6AB_2O_4 + 2B_B^x + \frac{3}{2}O_2 \rightleftharpoons 2V_B''' + 6h^\bullet + B_2O_3 \quad (22)$$

$$\frac{1}{2}O_2 + V_I^x \rightleftharpoons O_I'' + 2h^\bullet \quad (23)$$

$$O_O^x \rightleftharpoons \frac{1}{2}O_2 + V_O^{\bullet\bullet} + 2e' \quad (24)$$

The above equations were written using Kröger-Vink notation[83]. The relevant NiO, Fe, FeO, Fe_2O_3, Cr_2O_3, CrO and ZnO total energies were calculated using the same DFT methodology as for the spinel phases. The results are summarized in Table III as well as in Fig. 5. The oxygen partial pressure was set to unity. In order to directly compare the reactions and determine preferential type the data in Fig. 5 was scaled to represent the same A, B and O non-stoichiometry, respectively. For the metal ions the non-stoichiometry was measured with respect to $\frac{y_X}{y_A+y_B+y_O}$, where X is either A or B and y_X is the mole or atomic fraction of each species. The corresponding measure for the oxygen content is $\frac{y_O}{y_A+y_B}$. The deviation from stoichiometry was arbitrarily set to 0.0001. Note that Table III contains the actual reaction energies. In order to predict the composition and defect structure as function of the thermodynamic conditions a thermodynamic model should be constructed from the defect chemistry reactions above, which may either be based on mass action laws or on more general free energy models such as employed in the CALPHAD methodology[84,85].

Nevertheless, it is possible to draw several qualitative conclusions pertaining to the defect types likely responsible for non-stoichiometry. First, Fig. 5 shows that Reaction 22 is exothermic for both Fe_3O_4 and $CrFe_2O_4$, which leads to B deficiency or equivalently A and O excess. These two systems are the only that contain both Fe^{2+} and Fe^{3+} ions. For the spinel compounds with only either Fe^{2+} or Fe^{3+} ions, the corresponding reaction energies are positive. This observation is consistent with the Fe-O phase diagram[79], which exhibits oxygen excess at high temperature. The calculations seem to suggest a higher degree of non-stoichimetry than present CALPHAD models[79], but it is important to remember that under the thermodynamic conditions used in the present analysis ($P_{O_2} = 1$), Fe_2O_3 would be the equilibrium phase rather than Fe_3O_4 and, consequently, the calculated large negative reaction energy is not surprising. Also, the $h^\bullet$ formed in reaction 22 are equivalent to Fe^{3+} ions, implying that formation of Fe^{3+} vacancies via Reaction 22 in fact increases the number of Fe^{3+} ions, which should be the case since it leads to oxidation.

Another observation is that Reactions 14 and 15 lead to B excess (or equivalently A deficiency) and they have negative energies for all compounds except for $CrFe_2O_4$. Since B excess involves metal vacancies for charge compensation, these reactions are also equivalent to oxygen excess. The most negative energies are obtained for $FeCr_2O_4$, $NiCr_2O_4$ and $ZnCr_2O_4$. Interestingly, for $FeCr_2O_4$ and $CrFe_2O_4$ there is also the possibility of Reactions 14 and 15 involving Fe_2O_3 since Fe ions are mixed valent and appear as both Fe^{2+} and Fe^{3+}. The Fe_2O_3 based reactions have lower energies than the Cr_2O_3 based reactions, which implies that the oxidized spinel phases are more likely to be Fe rich than Cr rich. These results are at least partially consistent with phase diagram data. For example, the $NiFe_2O_4$[79] phase field extends all the way to Fe_2O_3 at high temperature and the $NiCr_2O_4$ phase field is Cr rich at high temperature[86]. We were unable to find any conclusive data for the other Cr spinel compounds. Since the calculations predict rather low reaction energies for many of the spinel compounds it would be interesting to explore this part of the phase diagram in more detail using either more advanced modeling of the finite temperature properties or by performing experiments. Note that the present simulations assume low defect concentrations and, even though the negative reaction energies suggest large non-stoichiometry, interaction among defects at higher concentrations may influence these properties.

From an oxygen non-stoichoiemtry perspective Reactions 14 and 15 have the lowest energies in the hyperstoichiometric regime, which implies that metal vacancies and in particular B vacancies are the preferred defect type. For $FeCr_2O_4$ and $CrFe_2O_4$ the Fe based version of these reactions are even lower in energy, as mentioned above. In the hypostoichimetric regime metal interstitials (Reaction 10) are the most favorable defect type, but in many cases oxygen vacancies formed via Reaction 24 are rather close in energy. This is in particular true for Fe_3O_4, which exhibits almost equal concentrations of Fe^{2+} and oxygen vacancies. Diffusion experiments have shown that metal vacancies and interstitials are responsible for the non-stoichiometry reactions in the hyperstoichiometric and hypostoichiometric regimes, respectively, for Fe_3O_4[87–90] and $(Cr_xFe_{1-x})_{3-\delta}O_4$[91]. These observations are consistent with our DFT calculations.

IV. CONCLUSIONS

Density functional theory (DFT) calculations were used to investigate the electronic, magnetic and thermodynamic properties of Fe-Ni-Cr-Zn spinel oxides, in particular all the pseudo-binary mixing energies and the formation energies of non-stoichiometric compounds were calculated. $NiFe_2O_4$-$ZnFe_2O_4$ exhibits a miscibility gap across the full composition range. $NiFe_2O_4$ dissolves $NiCr_2O_4$ up until Cr ions have filled all tetrahedral sites ($NiCrFeO_4$), after which the spinels exhibit a miscibility gap. Fe_3O_4-$FeCr_2O_4$ behaves in a similar way with Fe^{3+} ions easily replacing half of the Cr ions in $FeCr_2O_4$ thus forming $CrFe_2O_4$. The remaining Fe_3O_4-$CrFe_2O_4$ part of the phase diagram exhibits a miscibility gap. The predicted solution properties of Fe_3O_4-$NiFe_2O_4$ and Fe_3O_4-$FeCr_2O_4$ are consistent with the phases observed in corrosion of stainless steels.

There are a few exothermic (spontaneous) non-stoichimetry reactions in Fe-Ni-Cr-Zn spinel oxides. Among these, the reaction involving excess of trivalent B ions via B ions on A sites that are charge compensated by B vacancies has the most negative reaction energy according to the DFT calculations. This implies that oxy-

	Anti-site	Frenkel (A^{2+})	Frenkel (B^{3+})	Frenkel (O^{2-})	Schottky
Fe_3O_4	N/A	1.87	3.97	4.49	6.20
$NiFe_2O_4$	N/A	4.09	6.79	6.14	10.15
$ZnFe_2O_4$	0.14	4.00	3.00	6.35	11.13
$NiCr_2O_4$	1.12	3.20	4.53	7.57	19.42
$FeCr_2O_4$	3.31	3.39	4.81	7.03	16.58
$ZnCr_2O_4$	2.88	3.96	4.97	8.67	18.20
$CrFe_2O_4$	2.19	3.59	3.18	6.64	8.81

TABLE II. The intrinsic Frenkel and Schottky defect formation energies (Eqs. 3, 4, 5 and 6).

Reaction	Fe_3O_4	$NiFe_2O_4$	$ZnFe_2O_4$	$FeCr_2O_4$	$NiCr_2O_4$	$ZnCr_2O_4$	$CrFe_2O_4$
7	1.04	2.20	2.52	6.51	9.42	14.06	5.70
8	4.14	9.03	10.01	12.97	12.80	14.73	7.51
9	4.39	6.39	6.79	6.45	5.98	8.27	6.43
10	3.56	5.09	5.36	7.97	8.51	8.84	5.24
10c	3.56	5.32	8.20	6.65	5.65	7.30	5.33
11	1.98	3.85	3.32	4.48	4.58	5.14	7.53
12	9.43	9.72	8.86	8.05	5.80	7.47	1.33
13	-2.42	1.11	1.17	-0.37	0.28	0.25	3.79
13c	-2.42	1.68	1.55	0.24	0.68	0.86	-0.24
14	-0.10	0.59	-2.01	-7.70/-15.96	-7.98	-6.51	5.15/-6.57
15	-1.13	-2.26	-7.10	-10.92/-24.55	-12.37	-8.08	1.29/-14.40
16	2.35	3.02	4.24	-1.51	-2.41	0.67	4.36
17	N/A	-0.0032	-1.33	-1.05	-1.64	0.51	-1.14
18	8.49	8.31	8.62	8.23	7.08	10.35	9.21
19	7.68	6.36	6.90	10.51	10.87	11.20	8.14
19c	7.68	5.78	6.07	9.51	6.34	8.41	8.17
20	2.22	4.27	3.98	7.74	8.47	8.66	3.59
21	2.07	4.51	5.01	6.49	6.40	7.36	3.75
22	-4.29	0.03	0.76	0.47	2.02	0.64	-2.58
22c	-4.29	0.99	1.43	0.34	1.89	2.02	-3.41
23	0.15	3.40	3.96	2.44	3.06	4.18	2.59
23c	0.15	1.35	2.14	1.27	1.14	2.63	1.24
24	3.95	4.85	4.97	8.80	9.89	9.62	5.13
24c	4.10	4.31	5.46	5.51	5.54	4.87	3.95

TABLE III. Non-stoichiometry reactions in Fe_3O_4, $NiFe_2O_4$, $ZnFe_2O_4$, $NiCr_2O_4$ and $FeCr_2O_4$ spinel phases. For $FeCr_2O_4$ and $CrFe_2O_4$ the second value for Reactions 14 and 15 correspond to $B_2O_3 = Fe_2O_3$.

gen hyperstoichiometry primarily occurs via metal vacancies. Oxygen hypostoichiometry occurs via metal interstitials, but in many cases oxygen vacancies are rather close in energy. Both the metal interstitial and oxygen vacancy reactions are endothermic.

V. ACKNOWLEDGEMENTS

This work was supported by the Consortium for Advanced Simulation of Light Water Reactors (CASL) program of the US DOE Office of Nuclear Energy.

[1]

[2] 08 (1).

[3] E. J. W. Verwey, Nature **144**, 327 (1939).

[4] T. Sato, T. Iijima, M. Seki, and N. Inagaki, Journal of Magnetism and Magnetic Materials **65**, 252 (1987).

[5] R. H. Kodama and A. E. Berkowitz, Phys. Rev. B **59**, 6321 (1999), URL `http://link.aps.org/doi/10.1103/`

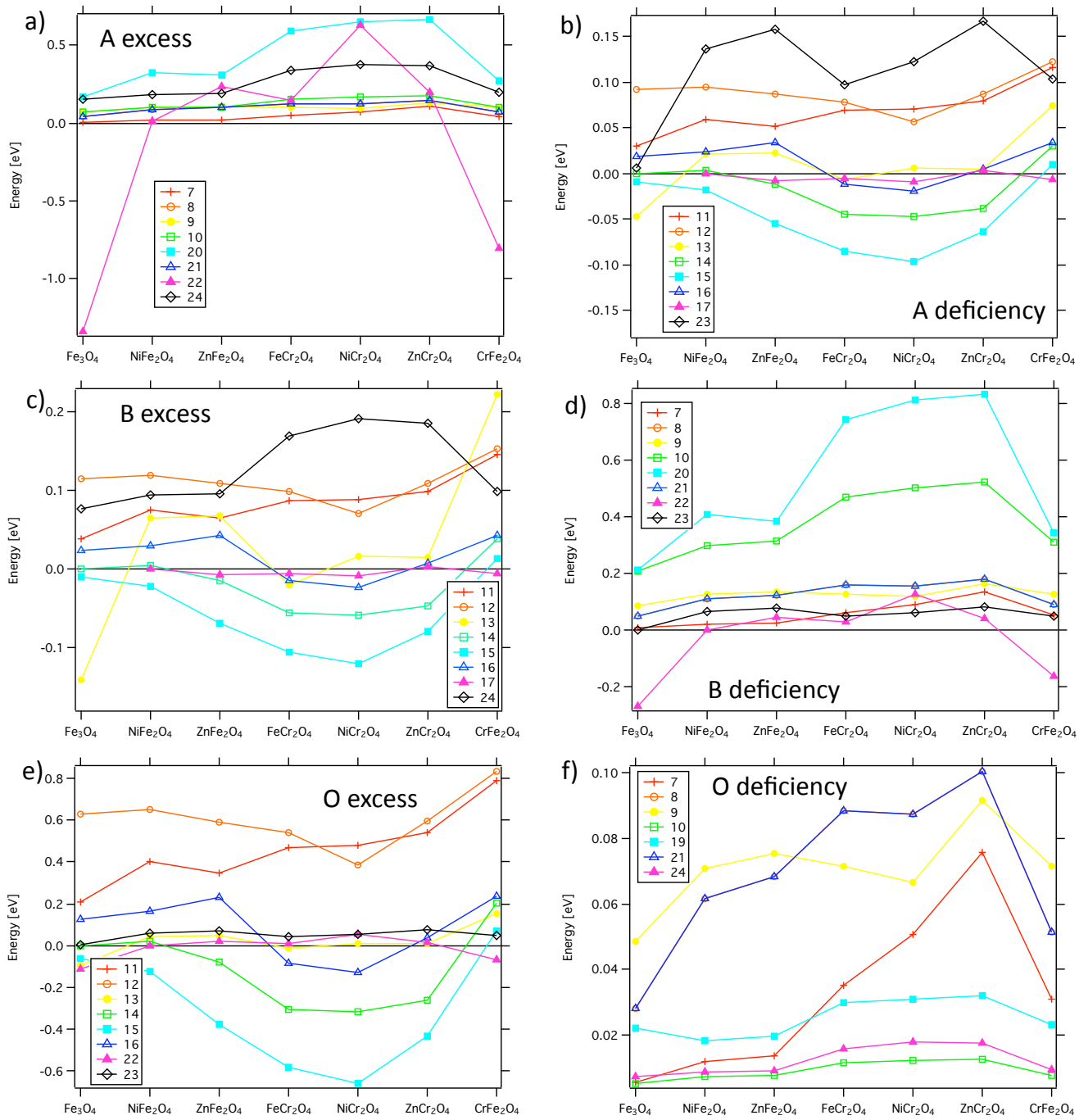

FIG. 5. The scaled non-stoichiometry reaction energies for a) A excess, b) A deficiency, c) B excess, d) B deficiency, e) O excess and b) O deficiency.

PhysRevB.59.6321.

[6] U. Lüders, G. Herranz, M. Bibes, K. Bouzehouane, E. Jacquet, J.-P. Contour, S. Fusil, J.-F. Bobo, J. Fontcuberta, A. Barthélémy, et al., J. Appl. Phys. **99**, 08K301 (2006).

[7] U. Lüders, A. Barthélémy, M. Bibes, K. Bouzehouane, S. Fusil, E. Jacquet, J.-P. Contour, J.-F. Bobo, J. Fontcuberta, and A. Fert, Advanced Materials **18**, 1733 (2006).

[8] N. W. Grimes, Phys. Technol. **6**, 22 (1975).

[9] G. P. Sabol, J. R. Secker, J. Kormuth, H. Kunishi, and D. L. Nuhfer, EPRI Report **TR-108320** (1997).

[10] G. P. Sabol, J. R. Secker, H. Kunishi, and B. Cheng, Proceedings of the Fontevraud IV SFEN/ENS International Symposium on Contribution of Materials Investigation to Resolution of Problems in Pressurized Water Reactors **2**, 1159 (1998).

[11] J. Henshaw, J. C. McGurk, H. E. Sims, A. Tuson, S. Dickinson, and J. Deshon, J. Nucl. Mater. **353**, 1 (2006).

[12] P. Tartaj, M. P. Morales, T. Gonzalez-Carreño, S. Veintemillas-Verdaguer, and C. J. Serna, Advanced Materials **23**, 5243 (2011).
[13] H. Zheng, J. Wang, S. E. Loand, Z. Ma, L. Mohaddes-Ardabili, T. Zhao, L. Salamanca-Riba, S. R. Shinde, S. B. Ogale, F. Bai, et al., Science **303**, 661 (2004).
[14] F. Zavaliche, H. Zheng, L. Mohaddes-Ardabili, S. Y. Yang, Q. Zhan, P. Shafer, E. Reilly, R. Chopdekar, Y. Jia, P. Wright, et al., Nano Letters **5**, 1793 (2005).
[15] N. Dix, V. Skumryev, V. Laukhin, L. Fàbrega, F. Sánchez, and J. Fontcuberta, Mat. Sci. Eng., B **144**, 127 (2007).
[16] R. Muralidharan, N. Dix, V. Skumryev, M. Varela, F. Sánchez, and J. Fontcuberta, J. Appl. Phys. **103**, 07E301 (2008).
[17] M. G. Chapline and S. X. Wang, Phys. Rev. B **74**, 014418 (2006).
[18] A. V. Ramos, T. S. Santos, G. X. Miao, M.-J. Guittet, J.-B. Moussy, and J. S. Moodera, Phys. Rev. B **78**, 180402 (2008).
[19] Y. Suzuki, Annu. Rev. Mater. Res. **31**, 265 (2001).
[20] U. Lüders, M. Bibes, J.-F. Bobo, M. Cantoni, R. Bertacco, and J. Fontcuberta, Phys. Rev. B **71**, 134419 (2005).
[21] S. Zhou, K. Potzger, Q. Xu, K. Kuepper, G. Talut, D. Markó, A. Mücklich, M. Helm, J. Fassbender, E. Arenholz, et al., Phys. Rev. B **80**, 094409 (2009).
[22] G. Kresse and J. Hafner, Phys. Rev. B **48**, 13115 (1993).
[23] G. Kresse and J. Furthmüller, Comp. Mater. Sci. **6**, 15 (1996).
[24] G. Kresse and J. Furthmüller, Phys. Rev. B **54**, 11169 (1996).
[25] G. Kresse and D. Joubert, Phys. Rev. B **59**, 1758 (1999).
[26] P. E. Blöchl, Phys. Rev. B **50**, 17953 (1994).
[27] J. P. Perdew, K. Burke, and M. Ernzerhof, Phys. Rev. Lett. **77**, 3865 (1996).
[28] P. Liao and E. A. Carter, J. Mater. Chem. **20**, 6703 (2010).
[29] V. N. Antonov, B. N. Harmon, and A. N. Yaresko, Phys. Rev. B **67**, 024417 (2003).
[30] A. Walsh, S.-H. Wei, Y. Yan, M. M. Al-Jassim, J. A. Turner, M. Woodhouse, and B. A. Parkinson, Phys. Rev. B **76**, 165119 (2007).
[31] D. Fritsch and C. Ederer, Phys. Rev. B **82**, 104117 (2010).
[32] G. S. Parkinson, T. A. Manz, Z. Novotný, P. T. Sprunger, R. L. Kurtz, M. Schmid, D. S. Sholl, and U. Diebold, Phys. Rev. B **85**, 195450 (2012).
[33] S. Soliman, A. Elfalaky, G. H. Fecher, and C. Felser, Phys. Rev. B **83**, 085205 (2011).
[34] C. Cheng, Phys. Rev. B **78**, 132403 (2008).
[35] Z. Szotek, W. M. Temmerman, D. Ködderitzsch, A. Svane, L. Petit, and H. Winter, Phys. Rev. B **74**, 174431 (2006).
[36] A. Jain, G. Hautier, S. P. Ong, C. J. Moore, C. C. Fischer, K. A. Persson, and G. Ceder, Phys. Rev. B **84**, 045115 (2011).
[37] K. T. Chan, J. D. Sau, P. Zhang, and M. L. Cohen, Phys. Rev. B **75**, 054304 (2007).
[38] C. J. Fennie and K. M. Rabe, Phys. Rev. Lett. **96**, 205505 (2006).
[39] D. J. Huang, C. F. Chang, H.-T. Jeng, G. Y. Guo, H.-J. Lin, W. B. Wu, H. C. Ku, A. Fujimori, Y. Takahashi, and C. T. Chen, Phys. Rev. Lett. **93**, 077204 (2004).
[40] G. S. Parkinson, T. A. Manz, Z. Novotný, P. T. Sprunger, R. L. Kurtz, M. Schmid, D. S. Sholl, and U. Diebold, Phys. Rev. B **85**, 195450 (2012).
[41] V. I. Anisimov, J. Zaanen, and O. K. Andersen, Phys. Rev. B **44**, 943 (1991).
[42] V. I. Anisimov, I. V. Solovyev, M. A. Korotin, M. T. Czyżyk, and G. A. Sawatzky, Phys. Rev. B **48**, 16929 (1993).
[43] I. V. Solovyev, P. H. Dederichs, and V. I. Anisimov, Phys. Rev. B **50**, 16861 (1994).
[44] S. L. Dudarev, D. N. Manh, and A. P. Sutton, Phil. Mag. **75**, 613 (1997).
[45] S. L. Dudarev, G. A. Botton, S. Y. Savrasov, C. J. Humphreys, and A. P. Sutton, Phys. Rev. B **57**, 1505 (1998).
[46] G. C. Zhou, L. Z. Sun, J. B. Wang, X. L. Zhong, and Y. C. Zhou, Physica B **403**, 2832 (2008).
[47] G. C. Zhou, L. Z. Sun, X. L. Zhong, S. X. Chen, W. Lu, and J. B. Wang, Phys. Lett. A **368**, 112 (2007).
[48] N. J. Mosey, P. Liao, and E. A. Carter, J. Chem. Phys. **129**, 014103 (2008).
[49] L. Wang, T. Maxisch, and G. Ceder, Phys. Rev. B **73**, 195107 (2006).
[50] H. J. Monkhorst and J. D. Pack, Phys. Rev. B **13**, 5188 (1976).
[51] P. E. Blöchl, O. Jepsen, and O. K. Andersen, Phys. Rev. B **49**, 16223 (1994).
[52] S. Lany and A. Zunger, Phys. Rev. B **78**, 235104 (2008).
[53] C. Persson, Y.-J. Zhao, S. Lany, and A. Zunger, Phys. Rev. B **72**, 035211 (2005).
[54] K. E. Sickafus, J. M. Wills, and N. W. Grimes, J. Am. Chem. Soc. **82**, 3279 (1999).
[55] W. H. Bragg, Nature **95**, 561 (1915).
[56] J. P. Wright, J. P. Attfield, and P. G. Radaelli, Phys. Rev. B **66**, 214422 (2002).
[57] A. Zunger, S.-H. Wei, L. G. Ferreira, and J. E. Bernard, Phys. Rev. Lett. **65**, 353 (1990).
[58] S.-H. Wei, L. G. Ferreira, J. E. Bernard, and A. Zunger, Phys. Rev. B **42**, 9622 (1990).
[59] C. Jiang, K. E. Sickafus, C. R. Stanek, S. P. Rudin, and B. P. Uberuaga, Phys. Rev. B **86**, 024203 (2012).
[60] C. Kittel, *Introduction to Solid State Physics* (Wiley, New York, USA, 2005), 8th ed.
[61] F. Grenveld and A. Sveen, J. Chem. Thermodyn. **6**, 859 (1974).
[62] S. E. Ziemniak, A. R. Gaddipati, P. C. Sander, and S. B. Rice, J. Phys. Chem. Solids **68**, 1476 (2007).
[63] D. J. Singh, M. Gupta, and R. Gupta, Phys. Rev. B **63**, 205102 (2001).
[64] S. E. Dutton, Q. Huang, O. Tchernyshyov, C. L. Broholm, and R. J. Cava, Phys. Rev. B **83**, 064407 (2011).
[65] G. Shirane, D. E. Cox, and S. J. Pickart, J. Appl. Phys. **35**, 954 (1964).
[66] H. Ishibashi and T. Yasumi, J. Magn. Magn. Mater. **310**, e610 (2007).
[67] J. B. Goodenough, Prog. Solid State Chem. **5**, 145 (1971).
[68] H. Perron, T. Mellier, C. Domain, J. Roques, E. Simoni, R. Drot, and H. Catalette, J. Phys.: Condens. Matter **19**, 346219 (2007).
[69] I. Leonov, A. N. Yaresko, V. N. Antonov, and V. I. Anisimov, Phys. Rev. B **74**, 165117 (2006).
[70] O. Kubaschewski, C. B. Alcock, and P. J. Spencer, *Materials Thermochemistry* (Pergamom Press, Oxford, 1993).
[71] M. Iizumi, T. F. Koetzle, G. Shirane, S. Chikazumi, M. Matsui, and S. Todo, Acta Cryst. B **38**, 2121 (1982).
[72] E. W. Gorter, Philips Res. Repts. **9**, 295 (1954).
[73] F. Braestrup, B. C. Hauback, and K. K. Hansen, J. Solid State Chem. **181**, 2364 (2008).

[74] G. Ueno, S. Sato, and Y. Kino, Acta Cryst. C **55**, 1963 (1999).
[75] W. D. Derbyshire and H. J. Yearian, Phys. Rev. **112**, 1603 (1958).
[76] H. S. C. O´ Neill and A. Navrotsky, Am. Miner. **68**, 181 (1983).
[77] S. Ziemniak, A. Gaddipati, and P. Sander, J. Phys. Chem. Solids **66**, 1112 (2005).
[78] B.-H. Park and D. Kim, Bull. Korean Chem. Soc. **20**, 939 (1999).
[79] L. Kjellqvist, M. Selleby, and B. Sundman, CALPHAD **32**, 577 (2008).
[80] R. Bauch, M. Cambini, P. Weisgerber, C. DeAsmundis, and C. Plog, J. Nucl. Mater. **92**, 334 (1980).
[81] J. Robertson, Corros. Sci. **29**, 1275 (1989).
[82] K. Kruska, S. Lozano-Perez, D. W. Saxey, T. Terachi, T. Yamada, and G. D. W. Smith, Corros. Sci. **63**, 225 (2012).
[83] F. A. Kröger and H. J. Vink, *Solid State Physics - Advances in Research and Applications* (Academic Press, New York, 1957).
[84] L. Kaufman and H. Bernstein, *Computer Calculation of Phase Diagrams* (Academic Press, New York, 1970).
[85] L. Kaufman and H. Bernstein, *CALPHAD Calculation of the Phase Diagram: A Comprehensive Guide* (Pergamon Press, London, 1998).
[86] A. D. Pelton, H. Schmalzried, and H. Sticher, J. Phys. Chem. Solids **40**, 1103 (1979).
[87] R. Dieckmann, Ber. Bunsenges. Physik. Chem. **86**, 112 (1982).
[88] R. Dieckmann, C. A. Witt, and T. O. Mason, Ber. Bunsenges. Physik. Chem. **87**, 495 (1983).
[89] R. Dieckmann and H. Schmalzried, Ber. Bunsenges. Physik. Chem. **81**, 344 (1977).
[90] R. Dieckmann, T. O. Mason, J. D. Hodge, and H. Schmalzried, Ber. Bunsenges. Physik. Chem. **82**, 778 (1978).
[91] J. Topfer, S. Aggarwal, and R. Dieckmann, Solid State Ion. **81**, 251 (1995).